Research Article | Vol. 24, No. 15 | 25 Jul 2016 | OPTICS EXPRESS 16799

Optics EXPRESS

Hybrid optical CDMA-FSO communications network under spatially correlated gamma-gamma scintillation

ANTONIO JURADO-NAVAS,[1,2,*] THIAGO R. RADDO,[1,3] JOSÉ MARÍA GARRIDO-BALSELLS,[2] BEN-HUR V. BORGES,[3] JUAN JOSÉ VEGAS OLMOS,[1] AND IDELFONSO TAFUR MONROY[1]

[1]*Dpt. Photonics Engineering, Technical University of Denmark (DTU), Akademivej Building 358, 2800 Kgs. Lyngby, Denmark*
[2]*Department of Communications Engineering, University of Málaga, Campus de Teatinos s/n, 29071 Málaga, Spain*
[3]*Department of Electrical and Computer Engineering, EESC, University of São Paulo (USP), 13560-250 São Carlos-SP, Brazil*
[*]*navas@ic.uma.es*

Abstract: In this paper, we propose a new hybrid network solution based on asynchronous optical code-division multiple-access (OCDMA) and free-space optical (FSO) technologies for last-mile access networks, where fiber deployment is impractical. The architecture of the proposed hybrid OCDMA-FSO network is thoroughly described. The users access the network in a fully asynchronous manner by means of assigned fast frequency hopping (FFH)-based codes. In the FSO receiver, an equal gain-combining technique is employed along with intensity modulation and direct detection. New analytical formalisms for evaluating the average bit error rate (ABER) performance are also proposed. These formalisms, based on the spatially correlated gamma-gamma statistical model, are derived considering three distinct scenarios, namely, uncorrelated, totally correlated, and partially correlated channels. Numerical results show that users can successfully achieve error-free ABER levels for the three scenarios considered as long as forward error correction (FEC) algorithms are employed. Therefore, OCDMA-FSO networks can be a prospective alternative to deliver high-speed communication services to access networks with deficient fiber infrastructure.

OCIS codes: (010.1330) Atmospheric turbulence; (290.5930) Scintillation; (060.1155) All-optical networks.

References and links

1. T. R. Raddo, A. L. Sanches, I. T. Monroy, and B.-H. V. Borges, "Throughput performance evaluation of multiservice multirate OCDMA in flexible networks," IEEE Photon. J. **8**, 1–15 (2016).
2. A. L. Sanches, T. R. Raddo, J. V. dos Reis, Jr., and B.-H. V. Borges, "Performance analysis of single and multirate FFHOCDMA networks based on PSK modulation formats," J. Opt. Commun. Netw. **7** 1084–1097 (2015).
3. J. V. dos Reis, Jr., T. R. Raddo, A. L. Sanches, and B.-H. V. Borges, "Fuzzy logic control for the mitigation of environmental temperature variations in OCDMA networks," J. Opt. Commun. Netw. **7** 480–488 (2015).
4. K. Kazaura, K. Wakamori, M. Matsumoto, T. Higashino, K. Tsukamoto, and S. Komaki, "RoFSO: a universal platform for convergence of fiber and free-space optical communication networks," IEEE Comm. Mag. **48**, 130–137 (2010).
5. L. C. Andrews and R. L. Phillips, and C.Y. Hopen, *Laser Beam Propagation through Random Media* (SPIE, 2005).
6. A. Jurado-Navas, A. Tatarczak, X. Lu, J. J. Vegas Olmos, J. M. Garrido-Balsells, and I. Tafur Monroy, "850-nm hybrid fiber/free-space optical communications using orbital angular momentum modes," Opt. Express **23**, 33721–33732 (2015)
7. I. S. Ansari, F. Yilmaz, and M. Alouini, "Performance analysis of free-space optical links over Málaga ($\mathscr{M}$) turbulence channels with pointing errors," IEEE Wirel. Communications **15**, 91–102 (2016).
8. A. Jurado-Navas, J.M. Garrido-Balsells, M. Castillo-Vázquez, and A. Puerta-Notario, "An efficient rate-adaptive transmission technique using shortened pulses for atmospheric optical communications," Opt. Express **18**, 17346–17363 (2010).
9. J Wang, J. Y. Yang, I. M. Fazal, N. Ahmed, Y. Yan, H. Huang, Y. Ren, Y. Yue, S. Dolinar, M. Tur, and A. E. Willner, "Terabit free-space data transmission employing orbital angular momentum multiplexing," Nat. Photon.

#262820 http://dx.doi.org/10.1364/OE.24.016799
Journal © 2016 Received 8 Apr 2016; revised 17 May 2016; accepted 26 May 2016; published 15 Jul 2016

Optics EXPRESS

6, 488–496 (2012).
10. F. Xu, A. Khalighi, P. Causse, and S. Bourennane, "Channel coding and time-diversity for optical wireless links," Opt. Express **17**, 872–887 (2009).
11. H. Manor, and S. Arnon, "Performance of an optical wireless communication system as a function of wavelength," Appl. Opt. **42**, 4285–4294 (2003).
12. X. Zhu, and J.M. Kahn, "Free space optical communication through atmospheric turbulence channels," IEEE Trans. Commun. **50**, 1293–1300 (2002)
13. A. Jurado-Navas, and A. Puerta-Notario, "Generation of correlated scintillations on atmospheric optical communications," J. Opt. Commun. Netw. **1**(5), 452–462 (2009).
14. I. E. Lee, Z. Ghassemlooy, W. P. Ng, and A. Khalighi, "Green-inspired hybrid FSO/RF wireless backhauling and basic access signalling for next generation metrozones," in Proc. 2nd Int. Symposium on Environment-Friendly Energies and Applications (EFEA), pp. 230–236, Newcastle (England), June 2012.
15. G. Parca, A. Shahpari, V. Carrozzo, G. Tosi Beleffi, and A.J. Teixeira, "Optical wireless transmission at 1.6-tbit/s (16×100 Gbit/s) for next-generation convergent urban infrastructures," Opt. Engineering **52**, 116102 (2013).
16. E. Leitgeb, M. Loschnigg, U. Birnbacher, G. Schwarz, and A. Merdonig, "High reliable optical wireless links for the last mile access," in Proc. of 10th Anniversary Int. Conf. Transparent Optical Networks (2008), pp. 178–183.
17. W. S. Rabinovich, C. I. Moore, R. Mahon, P. G. Goetz, H. R. Burris, M. S. Ferraro, J. L. Murphy, L. M. Thomas, G. C. Gilbreath, M. Vilcheck, and M. R. Suite, "Free-space optical communications research and demonstrations at the U.S. Naval Research Laboratory," Appl. Opt. **54**, F189–F200 (2015)
18. H. T.T. Pham, P. V. Trinh, N. T. Dang, and A. T. Pham, "Secured relay-assisted atmospheric optical code-division multiple-access systems over turbulence channels," IET Optoelectronics **9**, 241–248 (2015).
19. T. Miyazawa, and I. Sasase, "BER performance analysis of spectral phase-encoded optical atmospheric PPM-CDMA communication systems," J. Lightwave Technol. **25**, 2992–3000 (2007).
20. N. T. Dang, and A. T. Pham, "Performance improvement of FSO/CDMA systems over dispersive turbulence channel using multi-wavelength PPM signaling," Opt. Express **20**, 26786–26797 (2012).
21. K. Sasaki, N. Minato, and T. Ushikubo, "First OCDMA experimental demonstration over free space and optical fiber link," in Proc. Optical Fiber Communication Conf. (OFC), San Diego, Feb. 2008.
22. K. Kazaura, K. Omae, T. Suzuki, M. Matsumoto, E. Mutafungwa, T. Murakami, K. Takahashi, H. Matsumoto, K. Wakamori, and Y. Arimoto, "Performance evaluation of next generation free-space optical communication system," IEICE Trans. Electron. **E90-C**, 381–388 (2007).
23. E. Ciaramella, Y. Arimoto, G. Contestabile, M. Presi, A. D'Errico, V. Guarino, and M. Matsumoto, "1.28 Terabit/s (32×40 Gb/s) WDM transmission ver a double-pass free space optical link," IEEE J. Sel. Areas Commun. **27**, 1639–1645 (2009).
24. I. S. Hmud, F. N. Hasoon, and S. Shaari, "Optical CDMA system parameters limitations for AND subtraction detection scheme under enhanced double weight (EDW) code based on simulation experiment," Optica Applicata **40**, 669 –676 (2010).
25. R. Papannareddy, and A. M. Weiner, "Performance comparison of coherent ultrashort light pulse and incoherent broad-band CDMA systems," IEEE Photonics Tech. Lett. **11**, 1683–1685 (1999).
26. M. Matsumoto, T. Kodama, S. Shimizu, R. Nomura, K. Omichi, N. Wada, and K. Kitayama, "40G OCDMA-PON system with an asymmetric structure using a single multi-port and sampled SSFBG encoder/decoders," IEEE J. Light. Technol. **32**, 1132–1143 (2014).
27. H. Fathallah, L. A. Rusch, and S. LaRochelle, "Passive optical fast frequency-hop CDMA communications system," IEEE J. Lightwave Technol. **17**, 397–405 (1999).
28. T. R. Raddo, A. L. Sanches, I. T. Monroy, and B.-H. V. Borges, "Multirate IP traffic transmission in flexible access networks based on optical FFH-CDMA," in Proc. Intern. Conf. on Commun. (ICC), Kuala Lumpur, Malaysia, 2016, to be published.
29. T. R. Raddo, A. L. Sanches, J. V. dos Reis, Jr., and B.-H. V. Borges, "A new approach for evaluating the BER of a multirate, multiclass OFFH-CDMA system," IEEE Commun. Letters **16**, 259–261 (2012).
30. Z. Chen, S. Yu, T. Wang, G. Wu, S. Wang, and W. Gu, "Channel correlation in aperture receiver diversity systems for free-space optical communications," J. Opt. **14**, 125710 (2012)
31. M.A. Al-Habash, L.C. Adrews, and R.L. Phillips, "Mathematical model for the irradiance probability density function of a laser beam propagating through turbulent media," Opt. Eng. **40,** 1554–1562 (2001).
32. A. Jurado-Navas, J. M. Garrido-Balsells, J. F. Paris, M. Castillo-Vázquez and A. Puerta-Notario, "General analytical expressions for the bit error rate of atmospheric optical communication systems," Opt. Lett. **36**, 4095–4097 (2011).
33. J. M. Garrido-Balsells, A. Jurado-Navas, J. F. Paris, M. Castillo-Vázquez, and A. Puerta-Notario, "Spatially correlated gamma-gamma scintillation in atmospheric optical channels," Opt. Express **22**, 21820–21833 (2014).
34. P.G. Moschopoulos, "The distribution of the sum of independent gamma random variables," Ann. Inst. Statist. Math. (Part A) **37**, 541–544 (1985).
35. M.S. Alouini, A. Abdi, M. Kaveh, "Sum of gamma variates and performance of wireless communication systems over Nakagami-fading channels," IEEE Trans. Vehic. Tech. **50**, 1471–1480 (2001).
36. A. L. Sanches, J. V. dos Reis, Jr., and B.-H. V. Borges, "Analysis of high-speed optical wavelength/time CDMA networks using pulse-position modulation and forward error correction techniques," J. Lightwave Technol. **27**,

Optics EXPRESS

5134–5144 (2009).
37. A. Brinton Cooper, J. B. Khurgin, S. Xu, and J. U. Kang"Phase and Polarization Diversity for Minimum MAI in OCDMA Networks," IEEE J. Sel. Top. Quantum Electron. **13**, 1386–1395 (2007).
38. Wolfram, http://functions.wolfram.com/
39. T. Ohtsuki, "Performance analysis of atmospheric optical PPM CDMA systems," J. Lightwave Technol. **21**, 406-–411 (2003).
40. A. Jurado-Navas, J.M. Garrido-Balsells, M. Castillo-Vázquez, and A. Puerta-Notario, "Closed-form expressions for the lower-bound performance of variable weight multiple pulse-position modulation optical links through turbulent atmospheric channels," IET Commun. **6**, 390–397 (2011).
41. L.E. Nelson, Z. Guodong, M. Birk, C. Skolnick, R. Isaac, Y. Pan, C. Rasmussen, G. Pendock, and B. Mikkelsen, "A robust real-time 100G transceiver with soft-decision forward error correction [Invited]," J. Opt. Commun. Netw. **4**, B131–B141 (2012).

1. Introduction

Optical code-division multiple-access (OCDMA) has been regarded as a prominent architecture in emerging flexible, robust and high capacity passive optical networks (PONs) that support integration of diversified data traffic types and increased bandwidth [1–3]. The success of this technology is mainly due its ability of sharing the underlying network resources among their users. As a result, a variety of networking applications such as interactive e-learning, e-health, video-on-demand, multiplayer on-line games, and 4K ultra HD video streaming have now become available to a larger number of people. Notwithstanding PONs are one of the most successful broadband access architectures being deployed worldwide, although their deployment in remote locations still pose some difficulties (such as geographical, site access rights, high cost, and so on).

On another note, free-space optical (FSO) networks have been considered as an attractive alternative to provide high-speed communication services where fiber infrastructure deployment is impractical or deficient [4]. FSO communication systems have received considerable research efforts over the past years [4–9] mainly due to their inherent potential transmission capacity (much higher than that offered by radio transmission technologies). Furthermore, their narrow beam widths along with their license-free operation (as opposed to license paid microwave systems) make FSO systems appropriate candidates for secure, high-data-rate, and cost-effective wide-bandwidth communications. However, both atmospheric turbulence-induced fading (usually called scintillation) and strong path-loss constitute the major impairments associated to those links, limiting the application of FSO communication systems to short-range links. Several techniques have been proposed in the literature to mitigate these issues, such as temporal diversity [10], wavelength diversity [11] and spatial diversity [12, 13]. However, wavelength diversity techniques are considered less effective for atmospheric optical communication systems since turbulence on link performance remains almost unchanged for all optical wavelengths [11]. Whilst temporal diversity usually requires a longer signal processing time. Hence, spatial diversity becomes an attractive candidate for FSO communication, being one of the most commonly adopted.

Despite the propagation issues mentioned above, FSO networks have been successfully applied in metro-access network extension [14], enterprise connectivity [6, 15], last mile access [16] and ship-to-ship and aircraft-to-ground communications [17]. More interestingly, FSO networks become especially more attractive when combined with OCDMA networks [18–20]. Thanks to OCDMA inherent spread spectrum feature, the physical bandwidth of the medium can be increased when multiplexing various information channels simultaneously with the use of spreading codes. OCDMA has also several other remarkable features, such as soft-capacity on-demand, high scalability and support for multirate as well as symmetric bandwidth support for up- and downlinks [1, 2, 20]. The use of coding schemes grants to OCDMA networks a higher level of data security and asynchronism if compared to other network technologies. Therefore, the combination of OCDMA and FSO systems not only improves the transmission

Optics EXPRESS

capacity and the security level of the system, it also helps preserve the major aspect of both technologies, namely asynchronous transmission operation. Moreover, it can be seen as a prospective solution to deliver high-bandwidth services to last-mile access networks where the provision of broadband technologies has not been feasible so far.

The first experimental demonstration of an OCDMA-FSO network was reported in [21], proving that this technology can be successfully implemented. In fact, this approach may become part of the well-known next-generation FSO system [4, 6, 22] which consists of transmitting an optical beam from a fiber termination point over the atmospheric channel. Afterwards, in the receiver side, the light will be directly coupled into an optical fiber core. Hence, the need to convert the optical signal from electrical to optical formats or vice-versa for transmitting or receiving through the atmospheric channel is removed. As a result, data rates as high as 1 Tb/s and beyond are possible to achieve [15, 23].

In this paper, a novel asynchronous OCDMA-FSO network architecture based on a FFH coding scheme is proposed as a hybrid solution for access networks. New analytical formalisms for evaluating the average bit error rate (ABER) performance are also proposed. These formalisms, based on the spatially correlated gamma-gamma statistical model for the FSO link, are derived considering three distinct scenarios, namely, uncorrelated and totally correlated (both considered as limiting cases) channels, and partially correlated channels (usually considered a more generic case). Although the first two scenarios are a particular case of the third, they help us to establish important parameters of this hybrid system. For instance, the uncorrelated channel allows us to estimate the maximum possible benefit with the spatial diversity technique, while the totally correlated channel can be thought of as a system with solely one receiver without any spatial diversity scheme.

In addition, the new ABER expressions are validated via Monte Carlo simulations. In all scenarios, an equal gain-combining (EGC) technique is employed for combining the received irradiance collected in each receiving aperture lens. The ABER performance evaluation of the OCDMA-FSO network clearly shows that for all three scenarios error-free transmission can be achieved by means of FEC algorithms.

To the best of the authors' knowledge, this is the first report on the performance of asynchronous hybrid OCDMA-FSO networks. This paper is organized as follows. Section 2 lays out the hybrid OCDMA-FSO network architecture featuring also the FFH coding process carried out in the OCDMA users' signals. Section 3, by its turn, describes the correlated scintillation effects on FSO channels as well as the spatial diversity reception technique. The analytical formalisms for new closed-form ABER expressions are derived in Section 4. Finally, Section 5 presents relevant results regarding the proposed network under three previously mentioned scenarios and some concluding remarks are presented in 6.

2. OCDMA-FSO network description

One of the main purposes of this paper is to propose a new solution to geographically remote access networks based on a combined OCDMA-FSO technology and assuming that a spatial diversity technique is implemented in the receiver side.

Initially, regarding only the optical fiber channel of this hybrid network, the OCDMA part is arranged in a star topology connecting all users to the multiple access channel via optical fibers, as illustrated in Fig. 1, where each user has a transmitter and receiver (blue blocks).

At each transmitter, as shown in Fig. 2(a), the data information bits from each user (purple block) are on-off keying (OOK) modulated (green block) using a broadband source (grey block). Incoherent broadband optical sources such as light-emitting diode (LED) and amplified spontaneous emission (ASE) have low cost and are normally employed for modulation [24, 25]. Sequentially, the optical signal is encoded simultaneously in sequential time slots and disjoint wavelength subbands by the OCDMA encoder (orange block). Figure 2(b) shows the result of

Optics EXPRESS

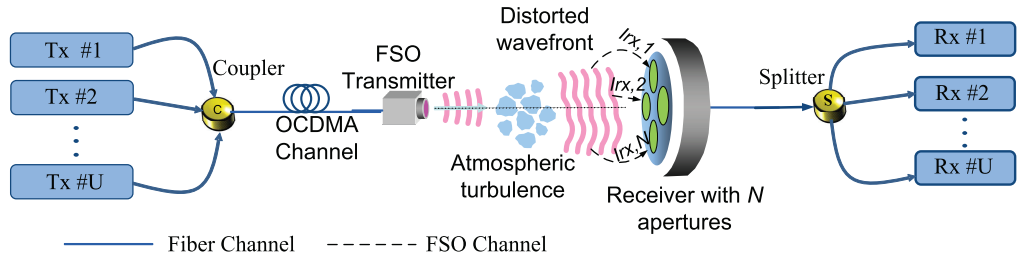

Fig. 1. Architecture of the hybrid OCDMA-FSO network connecting all U users in a star topology via optical fibers and a passive star coupler/splitter. In this Figure, Tx and Rx stand for transmitter and receiver, respectively.

the coding stage.

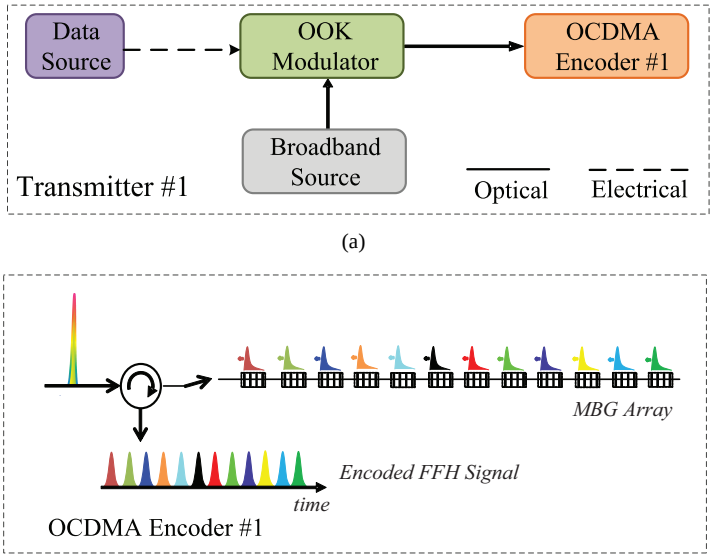

Fig. 2. (a) Block diagram associated to the OCDMA transmitter, showing its more important stages: the data source from each user, the OOK modulator, the broadband source and the OCDMA encoder. (b) OCDMA encoding process based on a MBG encoder.

Succeeding the code sequences assignment to users, the passive star coupler combines the output signals of the transmitters and provides access to the fiber channel as seen in Fig. 1. After being transmitted through the OCDMA channel, the desired user's signal arrives with multiple-access interference (MAI) at the free-space transmitter. Here, it is considered that all optical fiber non-idealities are appropriately compensated. Nonetheless, the simple superposition of users' signals in the star coupler produces MAI, which is delivered to each user by the splitter (at the fiber channel receiver side). Next, the signal is transmitted through the FSO channel, where signal attenuation/fading may occur due to absorption, scattering and scintillation. In fact, the turbulence-induced scintillation can affect both the signal intensity and phase, therefore deteriorating the transmitted signal. Despite it, the OCDMA network does not modify the signal phase since it employs incoherent modulation and encoding techniques where the intensity of an optical signal is encoded by unipolar codes.

Finally, at the receiver side, the FSO receiver collects the transmitted signal and a passive

Optics EXPRESS

star splitter delivers the signals to each user receiver. The OCDMA decoder then removes the temporal and wavelength translation introduced in the encoder [realigning the desired signal into a single pulse, see Figs. 3(a) and 3(b)]. After being decoded, the signal is directly detected by a photodetector (PD), where its electrical output signal is then integrated over the chip period (yellow block) under the suited time slot, and finally compared to a threshold level by a threshold decision device (green block). Accordingly, after these steps the signal recovery is finally completed. It is noteworthy that only the additional energy generated by the MAI within the chip period at which the autocorrelation peak is formed has an impact on the overall OCDMA network performance [2].

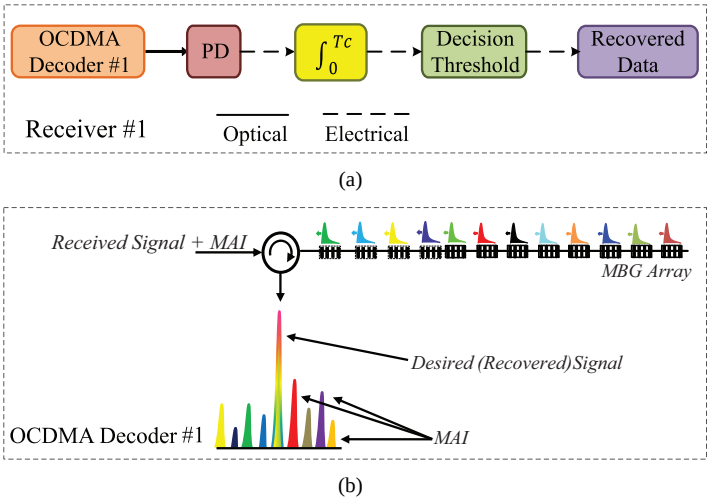

Fig. 3. (a) Block diagram of the OCDMA receiver employed for each user, showing its more important stages: the OCDMA decoder, the photodetector (PD), the integrator and decision threshold devices and, finally, the recovered data. (b) OCDMA decoding process based on a MBG (multiple Brag grating) decoder.

It is worth mentioning that feasible photodetectors with large bandwidths for data recovery are available for practical FFH-OCDMA network deployment as described in [26]. Furthermore, the encoders and decoders are composed of multiple Bragg gratings (MBGs)arrays [2, 27, 28]. The MBGs-based passive all-optical signal (de)coding allows practical implementation of FFH-based OCDMA networks. The gratings spectrally and temporally slice an incoming broadband pulse into several components generating FFH patterns according to a previously established code sequence. The Bragg gratings produce the frequency spectrum slicing whereas their spatial positions produce the respective time delays. On the other hand, the wavelengths at the decoder are positioned in reverse order with respect to the encoder in order to accomplish the matched filter decoding function. Interested readers should refer to [27] for further details on the passive optical FFH encoder/decoder.

Therefore, an exclusive code sequence with weight W and length L, in which each chip signaling slot occupies one wavelength, is assigned to each user. It is worth pointing out that in FFH-OCDMA networks changing L modifies the code weight W at the same instance [27, 29]. The total number of simultaneous users in the network is U and the chip duration of all users' codes is assumed constant and is given by $T_c = T_b/L$, where T_b is the bit period. Finally, without any loss of generality, deleterious noise sources such as optical channel impairments and time jitter are neglected since the main focus is on the MAI among the users' codes, generally considered as the dominant noise source in OCDMA networks [1, 2].

Optics EXPRESS

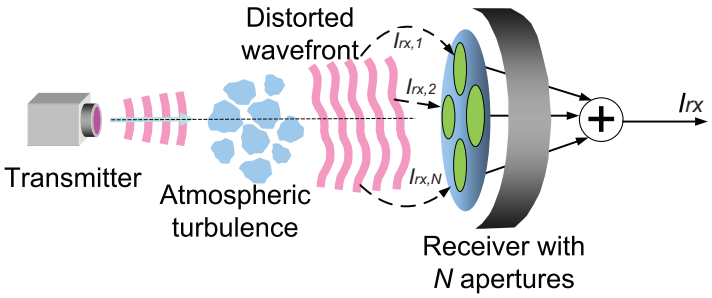

Fig. 4. Single-input multiple-output (SIMO) system model with a LED transmitter and N receiver apertures. All the irradiance contributions are added following an EQG technique.

3. Atmospheric spatially correlated channels

Atmospheric optical communication networks are receiving considerable attention recently in secure and high-speed transmissions. Normally, the propagation of the optical beam in FSO networks is affected due to fluctuations in both intensity and phase of the waves [5], even under clear sky conditions. Such turbulent process happens owing to the time varying inhomogeneities in the atmosphere refractive index. By its turn, the refractive index of the atmosphere changes as a direct consequence of temperature and pressure variations.

Consequently, a turbulent atmosphere may fade the optical beam irradiance propagated through FSO channels [5, 12, 13]. This turbulent-induced fading, also known as scintillation, degrades the average bit-error rate (BER), hence limiting FSO channels performance. Nevertheless, the spatial diversity reception technique [30] can be employed to mitigate these degrading effects since its spatial diversity redundancy enhances the FSO channel performance. Usually, the performance degradation is evaluated via the probability density function (PDF) of the irradiance. Among many irradiance PDF models available in the literature, one of the most accepted is the gamma-gamma (GG) one [5, 31], which considers the optical scintillation as a conditional random process [5, 31, 32].

A closed-form PDF expression for the sum of correlated GG distributed irradiances (at the FSO channel receiver side) considering both a spatial diversity reception with N apertures and an EGC diversity technique was derived in [33]. This spatial diversity reception is also considered here as illustrated in the FSO channel in Fig. 4.

Assuming OOK, IM/DD modulation and detection technique, and identical N aperture receiver lenses, the received optical irradiance, I_{rx}, can be expressed as a sum of the individual contributions received by every single receiver aperture as follows:

$$I_{rx} = \sum_{i=1}^{N} I_{rx,i} \tag{1}$$

Each individual contribution can be seen as a product of the irradiance ideal level that an aperture lens would receive in absence of atmospheric turbulence multiplied by a normalized irradiance component associated to the scintillation strength produced in the ith channel.

Without any loss of generality as well as for the sake of simplicity, the first component is considered equal to 1. The component I_{rx} denotes a GG random variable modeling the normalized irradiance observed by the ith receiver. As indicated in [5, 31], a GG normalized irradiance constitutes a modulated probability distribution function.

Accordingly, it consists of a doubly stochastic theory of scintillation, assuming that small scale irradiance fluctuations, Y_i, are modulated by large-scale irradiance fluctuations, X_i, of the propagating wave, both governed by independent gamma distributions. Then the irradiance can

Optics EXPRESS

be defined by $I_{rx,i} = X_i Y_i$, where both X_i and Y_i are defined by a gamma PDF. Further, it is considered that the same large eddies affect the signal received by the N receiver apertures as in [33]. Therefore, the large-scale component of scintillation is a common contribution for all of them, i.e., $X_i = X, \forall i = 1 \ldots N$. This case reflects the most unfavourable scenario for large-scale scintillation since the more uncorrelated the received signals are, the more efficient the spatial diversity technique is. On the contrary, the diffractive small-scale turbulence effect Y_i is dependent on each aperture, although it is assumed that all Y_i will be identically distributed. Hence, we can write Eq. (1) as follows:

$$I_{rx} = I = X \sum_{i=1}^{N} Y_i = XV, \tag{2}$$

where $V = \sum_{i=1}^{N} Y_i$, X follows a gamma distribution with parameters α_x and β_x, denoted as $X \sim \mathcal{G}(\alpha_x, \beta_x)$, and Y_i is characterized by parameters $\alpha_i = \alpha$ and $\beta_i = \beta$, i.e., $Y_i \sim \mathcal{G}(\alpha, \beta)$. Since I is a normalized optical irradiance, then $\alpha_x = 1/\beta_x$ and $\alpha = 1/(N\beta)$, respectively. Accordingly, $\mathrm{E}[I] = \mathrm{E}[X]\mathrm{E}[V] = 1$. Parameters α_x and α indicate the effective number of large-scale and small-scale eddies in the propagation path length, respectively, in the same manner as discussed in [31].

The inclusion of channel correlation implies the obtention of the PDF associated to the sum of correlated gamma random variables. To this end, a $N \times N$ correlation matrix, $\mathbf{C_y}$ is employed, given as:

$$\mathbf{C_y} = \begin{pmatrix} 1 & \rho_{12} & \cdots & \rho_{1N} \\ \rho_{21} & 1 & \cdots & \rho_{2N} \\ \vdots & \vdots & \ddots & \vdots \\ \rho_{N1} & \rho_{N2} & \cdots & 1 \end{pmatrix}, \tag{3}$$

with ρ_{ij} being the correlation coefficient depending on the distance between ith and jth receiver apertures.

As detailed in [33], by extending the Moschopoulos theorem [34] in the way proposed by Alouini et al. [35], it is possible to obtain the PDF of V. Then, the statistical distribution of the total received irradiance, I, can be directly obtained by averaging the latter PDF (seen as a conditional one) over the gamma distribution characterizing the variable X.

Since α represents the effective number of small scale turbulent eddies for each of the N receiving channels, it is a reasonable assumption to consider $\alpha \in \mathbb{N}$, and after some mathematical manipulations, it is possible to obtain the PDF of the combined received irradiance as

$$f_I(I) = \frac{2}{[\det(\mathbf{A})]^{\alpha}\Gamma(\alpha_x)} \sum_{i=1}^{N'} \sum_{m=1}^{\alpha_i} \frac{c_{mi}}{\Gamma(m)} \lambda_i^{\frac{m-\alpha_x}{2}} \alpha_x^{\frac{m+\alpha_x}{2}} I^{N\alpha-1-\frac{m-\alpha_x}{2}} K_{m-\alpha_x}\left(2\sqrt{\frac{\alpha_x I}{\lambda_i}}\right), \tag{4}$$

where $\{\lambda_i\}_{i=1}^{N}$ are the eigenvalues of the matrix $\mathbf{A} = \mathbf{DC}$, with $\mathbf{D}$ being a $N \times N$ diagonal matrix with the entries β for $i = 1 \ldots N$, whereas $\mathbf{C} = \sqrt{\mathbf{C_y}}$ is a $N \times N$ positive definite correlation matrix. Hence, $\det(\mathbf{A}) = \prod_{i=1}^{N} \lambda_i$. Moreover, N' denotes the number of different eigenvalues of matrix $\mathbf{A}$ and $\Gamma(\cdot)$ denotes the Gamma function whereas $K_\nu(\cdot)$ is the modified Bessel function of the second kind and order ν. Finally, c_{mi} is a coefficient depending on I arising from a partial

Optics EXPRESS

fraction expansion procedure, in the form:

$$c_{mi} = \frac{1}{(\alpha_i - m)!} \frac{\mathrm{d}^{\alpha_i - m}}{\mathrm{d}w^{\alpha_i - m}} \left[\prod_{\substack{j=1 \\ j \neq i}}^{N'} \frac{1}{(w - d_j)^{\alpha_j}} \right]_{w=d_i} = \\ = \frac{1}{(\alpha_i - m)!} \sum_{k_1 + \ldots + \hat{i} + k_{N'} = \alpha_i - m} \binom{\alpha_i - m}{k_1 \ldots \hat{i} \ldots k_{N'}} \times \prod_{\substack{j=i \\ j \neq i}}^{N'} \left[(-1)^{k_j} (\alpha_j)_{k_j} (d_i - d_j)^{-\alpha_j - k_j} \right], \tag{5}$$

where $\hat{i}$ indicates that k_j is omitted. On the other hand, $(\alpha_j)_{k_j}$ is the Pochhammer symbol, $d_i = -I/\lambda_i$, α_i is the product of the algebraic multiplicity of the eigenvalue, denoted as $\mu_A(\lambda_i)$, with the parameter α. Finally, the set of k_i coefficients arises from the multinomial theorem given by:

$$\frac{\mathrm{d}^n}{\mathrm{d}x^n} \left(\prod_{j=1}^{N} u_j \right) = (u_1 + \cdots + u_N)^{(n)} = \sum_{k_1 + \ldots + \hat{i} + k_{N'} = n} \binom{n}{k_1, \ldots k_N} \prod_{j=1}^{N} u_j^{(k_j)}, \tag{6}$$

and they are employed after calculating the generalized Leibniz rule, where the latter is required to obtain the c_{mi} coefficients. Finally, it is straightforward to obtain $u_j = (w - d_j)^{-\alpha_j}$.

4. OCDMA-FSO network performance evaluation

In this section, we derive a closed-form analytic expression for the bit error rate associated to a combined OCDMA-FSO network taking into account both turbulence-induced scintillation and MAI. Then we investigate the following network scenarios: totally correlated channels, partially correlated channels and completely uncorrelated channels. We start with the error probability of a conventional OCDMA system, which is then averaged by the PDF associated to the atmospheric optical channel.

4.1. OCDMA BER evaluation

This subsection deals with the BER evaluation of the FFH-based OCDMA network. This network employs an OOK intensity-modulated incoherent structure, where each user transmits its assigned code sequence for data bit "1" whereas no signal is transmitted for data bit "0".

There are several noise sources that affect the performance of OCDMA networks, such as time jitter, non-linear effects, channel impairments [36], temperature variation [3] and, certainly, MAI [37]. However, since MAI is usually the dominant noise component in such networks [1, 2] it is considered here as the only signal's degradation source in addition to the additive white Gaussian noise (AWGN). Notwithstanding the AWGN has no significant impact on the OCDMA performance, it may degrade the hybrid OCDMA-FSO network performance considerably due to the FSO link [8]. Thus, it is considered MAI and AWGN on the detection of the desired user's bit. Hence, the decision variable at the matched filter output becomes

$$Z = \int_0^{T_c} r(t) C_1(t) \mathrm{d}t = bW + I_I + \xi, \tag{7}$$

where $r(t)$ and $C_1(t)$ are, respectively, the received signal at the input of the decoder, and the encoded transmitted signal of the desired user. I_I denotes the total MAI given by the sum of the interferences from all users. Finally, $b \in \{0, 1\}$ is the binary data, W represents the code weigth whilst ξ is a zero-mean AWGN.

Optics EXPRESS

The FFH-based code employed here has maximum nonzero shift autocorrelation and cross-correlation bounded by one [2, 27, 29], and each interfering user contributes with only one chip overlapping on the desired user's code. It is assumed that transmissions among users are chip-synchronous, which reflects the worst possible scenario for the OCDMA performance analysis [28]. Now, the optimum threshold, μ, is set to $\mu = W + \eta$ [2], where $\eta = (U-1)\mathscr{P}$ is the MAI mean, with U representing the total number of simultaneous users in the network, with $\mathscr{P}$ being the probability of interference between the desired user and an interfering user defined as $\mathscr{P} = W^2/(2LF)$ [29], with F being the total number of available wavelengths. Then, considering that the transmission probabilities of bits "0" and "1" are equiprobable, the BER of the OCDMA network can be evaluated from the decision variable Z as [27]

$$\begin{aligned} P_b(e) =& P(Z \le \mu | b=0) \cdot P(b=0) + P(Z < \mu | b=1) \cdot P(b=1) \\ =& \frac{1}{2}\left[P(Z \le \mu | b=0) + P(Z < \mu | b=1)\right] = Q\left(\sqrt{\zeta}\right), \end{aligned} \tag{8}$$

where $Q(\cdot)$ is the well-known Q-function, ζ is the signal-to-interference ratio (SIR) of the OCDMA network that can be directly obtained as

$$\zeta = \frac{W^2}{(U-1)\sigma^2 + \sigma_N^2}, \tag{9}$$

with $\sigma^2 = (U-1)\mathscr{P}(1-\mathscr{P})$ denoting the MAI variance. Finally, σ_N^2 represents the additive white Gaussian noise (AWGN) variance characterizing ξ. Although MAI has a binomial distribution [28], the well-known $Q(\cdot)$ function is utilized here because the central limit theorem allows the MAI interference in single rate networks to be approximated by a Gaussian function as long as the number of simultaneous users are large enough [2, 27]. The BER performance analysis with additional deleterious noise sources will be published elsewhere.

4.2. OCDMA-FSO BER evaluation

This subsection presents the BER derivation of the hybrid OCDMA-FSO network considering both MAI and the atmospheric channel impairment effects. Then, since the FSO network has a random behavior related to the random turbulence conditions, it is necessary to average Eq. (8) over the irradiance PDF I. Thus, Eq. (8) becomes a conditional on the irradiance power and, from now onwards, is denoted as $P_b(e|I)$. The final BER expression is considered an average (ABER) denoted here as $P_b(e)$. Next, it is derived new $P_b(e)$ expressions considering three distinct scenarios based on the correlation degree among different received irradiance sequences. They are: (a) no correlation among small-scale fluctuations (considered the limiting case); (b) total correlation among small-scale scintillations (also considered as the limiting case); and the generic case of (c) partially correlated sequences associated to the received irradiance contributions.

4.2.1. No correlation among irradiance sequences in the FSO receiver side

When the turbulent small-scale effects associated to each channel are completely independent, the scenario is reduced to a single-input single-output (SISO) channel with $\mathbf{C_Y}$ becoming a diagonal correlation matrix. In this case, $X \sim \mathscr{G}(\alpha_x, \beta_x)$ and $V = \sum_{i=1}^{N} Y_i \sim \mathscr{G}(N\alpha, 1/(N\alpha))$ can be easily obtained from Eq. (2). Then, after substituting them into Eq. (4), the PDF of the received normalized irradiance becomes [33]:

$$f_I(I) = \frac{2(\alpha_x N\alpha)^{\left(\frac{N\alpha+\alpha_x}{2}\right)}}{\Gamma(N\alpha)\Gamma(\alpha_x)} I^{\frac{N\alpha+\alpha_x}{2}-1} K_{N\alpha-\alpha_x}\left(2\sqrt{\alpha_x N\alpha I}\right). \tag{10}$$

Optics EXPRESS

It is straightforward to note that Eq. (10) is the single GG PDF with X and V modeled by a gamma distribution whose shape parameters are, respectively, α_x and $N\alpha$. Subsequently, it is desired to average Eq. (10) over Eq. (8) to finally obtain the ABER of the OCDMA-FSO network. Thus, the BER conditioning on I, denoted as $P_b(e|I)$, becomes

$$P_b(e) = \int_0^\infty P_b(e|I)\, f_I(I) \mathrm{d}I. \tag{11}$$

Furthermore, the Q-function in Eq. (8) can be rewritten in terms of the complementary error function $\mathrm{erfc}(\cdot)$. Then, both the $\mathrm{erfc}(\cdot)$ and the modified Bessel integrands can be written as Meijer G functions using [38, Eqs. (07.34.03.0619.01) and (07.34.03.0605.01)]. Such expression is therefore rearranged as

$$G_{2,0}^{1,2}\left(z \middle| \begin{matrix} a \\ a-1, a-1/2 \end{matrix}\right) = \sqrt{\pi} z^{a-1} \mathrm{erfc}(\sqrt{z}). \tag{12}$$

$$G_{2,0}^{0,2}\left(z \middle| a, b\right) = 2z^{\frac{a+b}{2}} K_{a-b}\left(2\sqrt{z}\right). \tag{13}$$

One can finally derive the closed-form ABER expression, using [38, Eqs. (07.34.03.0619.01) and (07.34.03.0605.01)], as

$$P_b^{nc}(e) = \frac{2^{N\alpha+\alpha_x-1}}{2\pi\sqrt{\pi}\Gamma(N\alpha)\Gamma(\alpha_x)} G_{5,2}^{2,4}\left(\frac{8\zeta}{(\alpha_x N\alpha)^2} \middle| \begin{matrix} \frac{1-N\alpha}{2}, \frac{2-N\alpha}{2}, \frac{1-\alpha_x}{2}, \frac{2-\alpha_x}{2}, 1 \\ 0, \frac{1}{2} \end{matrix}\right), \tag{14}$$

where the signal-to-interference ratio, ζ, is given by Eq. (9).

4.2.2. Total Correlated Channels

This subsection deals with the BER derivation of the OCDMA-FSO network considering a total correlated channel scenario. This scenario, which consists of receiving N totally correlated small-scale irradiance fluctuations (in the receiver side) establishes the limiting case of the network as in the previous subsection.

Thus, assuming that all the transmitted power is collected by N apertures, it can be easily obtained from (2) that $V = \sum_{i=1}^{N} Y_i \sim \mathscr{G}(\alpha, 1/(\alpha))$. Then, the irradiance PDF follows a classic GG distribution [31], where α_x and α are, respectively, its large and small scale parameters. Adopting a similar procedure as in the previous subsection, the corresponding ABER expression becomes

$$P_b^{tc}(e) = \frac{2^{\alpha+\alpha_x-1}}{2\pi\sqrt{\pi}\Gamma(\alpha)\Gamma(\alpha_x)} G_{5,2}^{2,4}\left(\frac{8\zeta}{(\alpha_x\alpha)^2} \middle| \begin{matrix} \frac{1-\alpha}{2}, \frac{2-\alpha}{2}, \frac{1-\alpha_x}{2}, \frac{2-\alpha_x}{2}, 1 \\ 0, \frac{1}{2} \end{matrix}\right). \tag{15}$$

It can be noted from Eq. (15) that both cases (N totally correlated small-scale scintillations and a single-aperture receiver) are identical. Finally, the superindex tc denotes total correlation.

4.2.3. Partially correlated channels

In this subsection, the closed-form ABER expression of the OCDMA-FSO network is derived assuming partially correlated channels, which is usually the generic scenario. Then, considering realistic correlation coefficients ρ_{ij}, we can average Eq. (9) over Eq. (4) to solve Eq. (11), with the help of Eqs. (12) and (13) and [38, Eq. (07.34.21.0013.01)]. Hence, the ABER

Optics EXPRESS

corresponding to the case of partially correlation, $P_b^{pc}(e)$, can be written as

$$P_b^{pc}(e) = \frac{2}{[\det(\mathbf{A})]^{\alpha}\Gamma(\alpha_x)} \sum_{i=1}^{N'} \sum_{m=1}^{\alpha_i} \frac{1}{\Gamma(m)} \frac{\lambda^{\frac{m-\alpha_x}{2}} \alpha_x^{\frac{m+\alpha_x}{2}}}{(\alpha_i - m)!} \sum_{k_1+\ldots\overset{\hat{i}}{}+k_{N'}=\alpha_i-m} \binom{\alpha_i - m}{k_1 \ldots \overset{\hat{i}}{} \ldots k_{N'}}$$
$$\times \prod_{\substack{j=i \\ j\neq i}}^{N'} \left[(-1)^{k_j} (\alpha_j)_{k_j} \left(\frac{\lambda_j - \lambda_i}{\lambda_i - \lambda_j} \right)^{-\alpha_j - k_j} \right] 2^{\frac{-2\alpha_i - 2k_j + 2N\alpha - m + \alpha_x - 1}{4\pi^{3/2}}} \left(\frac{\alpha_x}{\lambda_i} \right)^{-\frac{(N\alpha - \alpha_i - k_j - \frac{m-\alpha_x}{2})}{2}}$$
$$\times G_{5,2}^{2,4}\left(\frac{8\zeta\lambda_i^2}{\alpha_x^2} \middle| \begin{matrix} \frac{1+\alpha_i+k_j-N\alpha}{2}, \frac{2+\alpha_i+k_j-N\alpha}{2}, \frac{1+\alpha_i+k_j-N\alpha+m-\alpha_x}{2}, \frac{2+\alpha_i+k_j-N\alpha+m-\alpha_x}{2}, 1 \\ 0, \frac{1}{2} \end{matrix} \right). \tag{16}$$

5. Results and discussions

The mathematical formalisms developed in the previous section are now applied to evaluate the performance of the OCDMA-FSO network for three scenarios, which are based on [2] and [33].

It is worth mentioning that the Monte Carlo simulations were carried out for all scenarios investigated in this section. The numerical simulations agreed perfectly with the analytical ones show here. Hence, they do demonstrate that the new proposed BER expressions are robust and accurate. Thus, consider an OCDMA-FSO network employing FFH-based codes [2, 29] with code length, code weight, number of wavelengths, and number of users given, respectively, by $W = 12$, $L = 12$, $F = 29$, and $U = 29$. The number of simultaneous interfering users considered here is large enough so that MAI can be accurately approximated as Gaussian distributed [2,27].

For this current network configuration, the MAI variance changes from 2.69 (14 users) to 4.59 (29 users) according to the number of simultaneous users in the network. In addition, it is considered two distinct schemes in the FSO channel, namely, a SISO channel and a single-input multiple-output scheme employing EGC spatial diversity technique with four aperture collecting lenses in the FSO receiver. In the latter scheme, it is assumed that the small-scale scintillation sequences are completely uncorrelated ($\rho_{ij} = 0\ \forall i \neq j$; $\rho_{ii} = 1$). The parameters related to the gamma-gamma FSO channel are listed in Table 1, which also includes the irradiance variance, σ_I^2, that affects the network.

Table 1. Atmospheric channel features.

α_x	α	σ_I^2 (N=1)	σ_I^2 (EGC N=4) ($\rho_{ij} = 0\ \forall i \neq j$, $\rho ii = 1 \forall i = 1 \ldots N$)	σ_I^2 (EGC N=4) ($\rho_{i,i+1} = 0.7$, $\rho_{i,i+2} = 0.5$, $\rho ii = 1$)
10	10	0.21	0.1276	0.1799
50	50	0.04	0.0251	0.0348
100	100	0.02	0.0125	0.0173
666	666	0.003	0.0019	0.0026

The average BER as a function of the number of simultaneous users is shown in Fig. 5. All curves are directly obtained from Eqs. (14) – (16). This figure shows that the ABER tends to worsen as the number of simultaneous users increases. This occurs due to the increased MAI variance and, consequently, to the SIR reduction according to Eq. (9). Nevertheless, when U tends to infinity, the limiting values of Eqs. (14) – (16) all tend to 0.5.

It can still be noted from Fig. 5 that the fading intensity variation of the FSO channel changes considerably the network performance. When the irradiance fluctuation variance, σ_I^2,

Optics EXPRESS

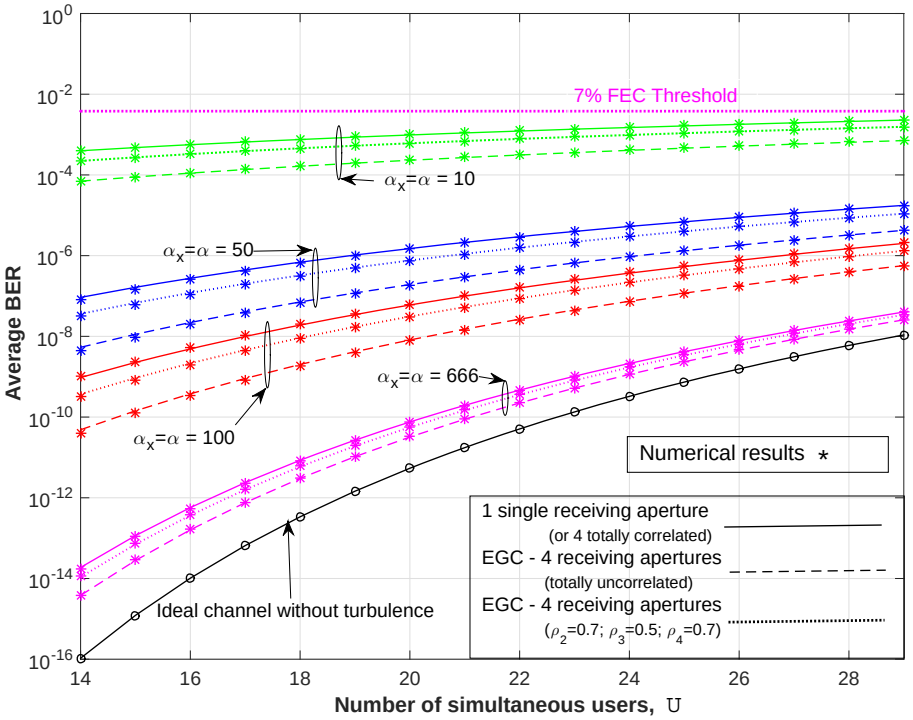

Fig. 5. Average BER performance associated to an OCDMA-FSO communication system for different number of active users as well as turbulence regimes. Two limiting cases are shown: a receiver with only one single receiving aperture lens (dotted line), and a receiver implementing EGC with 4 aperture collecting lenses and no correlation among the small-scale scintillation sequences (solid line). Furthermore, an example of partial correlation with $\rho_{12} = \rho_{14} = 0.7$ and $\rho_{13} = 0.5$ is also shown. Numerical results obtained by applying Monte Carlo simulation are also displayed (asterisk).

increases, the associated ABER decreases. For example, for the case of $N = 1$ (equivalent to the case of four totally correlated small-scale scintillations), and considering $U = 20$, we have obtained an associated ABER of 7.6×10^{-11}, for $\sigma_I^2 = 0.003$, whereas the ABER reduces to approximately 10^{-3} when $\sigma_I^2 = 0.21$. But remarkably it is still within the limit imposed by a forward error correction (FEC) technique (ABER $\leq 3.8 \times 10^{-3}$, see horizontal dotted line in Fig. 5). Therefore, even for the worst fading intensity case studied ($\alpha_x = \alpha = 10$), it is possible to accommodate all users in the error-free transmission regime when FEC is employed.

It can be further noted how the degree of correlation among channels influences the final performance of the OCDMA-FSO network. If we focus on the limiting cases (uncorrelated versus totally correlated small-scale fading), it is straightforward to extract the maximum benefit of this EGC spatial diversity technique. Hence, for $U = 14$, a received average BER of 7×10^{-5} and 4×10^{-5} for the cases of totally correlated and uncorrelated channels, respectively, are obtained for $\alpha_x = \alpha = 10$. However, these values reduce, respectively, to 1.88×10^{-14} and 3.81×10^{-15} for $\alpha_x = \alpha = 666$. Nevertheless, when the number of users increases to $U = 29$, the associated ABERs are 2.3×10^{-3} and 7.1×10^{-4}, respective to totally correlated channels and totally independent channels, with $\alpha_x = \alpha = 10$. On the other hand, the improvement is less relevant for the case of $\alpha_x = \alpha = 666$, which results in a BER of 4×10^{-8} and 2.5×10^{-8}, respective to total correlation and no correlation among small-scale scintillations. Finally, it can be concluded from Fig. 5 that the network has the best ABER performance under the ideal case,

Optics EXPRESS

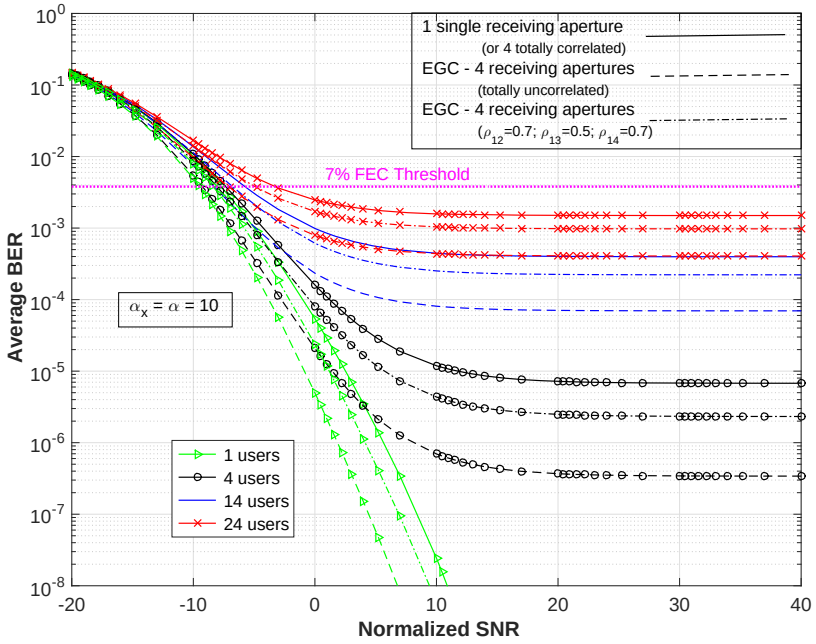

Fig. 6. Average BER performance associated to an OCDMA-FSO communication system with an EGC technique in the receiver side (4 aperture collecting lenses) for different number of active users in the system and a turbulence regime characterized by $\alpha_x = \alpha = 10$. Three cases are displayed depending on the degree of correlation among the received small-scale scintillation sequences: (a) total correlation (solid line), (b) no correlation (dashed line), and (c) partially correlated sequences (dashed-dotted line) with $\rho_{12} = 0.7, \rho_{13} = 0.5$, and $\rho_{14} = 0.7$.

when scintillation effects are not considered.

Subsequently, the ABER versus the SIR considering a weak-to-moderate turbulence regime is plotted in Fig. 6 for different number of simultaneous users in the OCDMA-FSO network ($U = 1, 4, 14$ and 24). The same three previously defined scenarios are again investigated. Since the numerical simulations agreed perfectly with the analytical results, they are not plotted in Fig. 6 for the sake of clarity.

As can be noticed from Fig. 6, as the number of simultaneous users increases, the ABER performance decreases for all three turbulence scenarios. The ABER performance reduction is even more evident when the number of users in larger than 1. For such case, considering SNR = 7 dB, for 4 simultaneous users (black lines) under the totally uncorrelated scenario, the ABER is approximately 2.8×10^{-5} whereas for 14 simultaneous users (blue lines) the ABER is reduced to approximately 5.4×10^{-4}. Accordingly, if the number of simultaneous users increases to $U = 24$ (red lines), the ABER decreases to 1.7×10^{-3}.

Notice further from Fig. 6 that there is an error floor in terms of ABER when more than 1 user is active in the network. Consequently, increasing the SNR after a certain level does not improve the ABER performance anymore. This is a well-known phenomenon induced by scintillation, as shown in [39, 40]. This effect is enhanced due to MAI present in OCDMA-FSO networks. Nevertheless, all simultaneous users can still obtain error-free transmissions (ABER $\leq 10^{-12}$) as long as FEC (with only 7 % of overhead) [41] is employed under a SNR as low as - 1 dB. Eventually, an ABER limit of 3.8×10^{-3} [41] for hard decision (see horizontal dotted line in Fig. 6) should be adopted to implement this FEC algorithm, thus representing the error-free transmission limit. Regarding coherent OCDMA-FSO networks, where the bit information is

Optics EXPRESS

encoded in the phase of an optical signal, the ABER performance may suffer serious deleterious effects due to phase variations, especially in the FSO channel. But this issue is beyond the scope of the present study and will be addressed in a future publication.

6. Concluding remarks

In this paper, we have presented and thoroughly described a hybrid solution based on OCDMA and FSO affected by MAI and correlated gamma-gamma atmospheric turbulence. The proposed architecture considers that users access the network in a fully asynchronous manner by means of assigned FFH-based codes. In addition, an EGC spatial diversity technique was employed in the FSO receiver side. Thus new analytical expressions to evaluate the network performance of this combined OCDMA-FSO system were derived.

We have investigated the limiting conditions for the system, which mainly depends on the correlation degree among small-scale fluctuations in the received irradiance sequences since large-scale component of scintillation is supposed to be a common contribution for all of them. Consequently, depending on that aforementioned correlation degree, we have established two limiting cases: (a) no correlation among small-scale fluctuations, as shown in Eq. (14); and (b) total correlation among small-scale scintillation sequences, as represented in Eq. (15). The former condition case, considered of great interest, allows one to estimate the maximum possible benefit of the EGC spatial diversity technique. Conversely, Eq. (15) allows the performance investigation of the network with only one larger FSO receiver aperture. Both equations represent in a simple expression the upper and lower bounds, respectively, of the EGC technique studied in this paper. In addition, we have derived a closed-form ABER expression, Eq. (16), for the general performance case, where the correlation coefficient between any pair of received sequences is from 0 to 1.

The obtained results show that both the presence of a turbulent medium and the consideration of MAI in the system constitute limiting factors degrading the behavior of the system in terms of ABER. In this sense, the stronger the intensity of the turbulence, the worse the ABER expected in the network. Furthermore, the combination of interfering users and turbulence plus MAI induces the presence of an error floor in the system that may be impossible to overcome, even if the AWGN power is totally removed from the system.. Fortunately, by including a hard decision forward error correction with 7 % overhead, it is possible to recover the transmitted information for all cases displayed in Fig. 6 (up to 24 users in the system in a weak-to-moderate turbulence regime) as long as the SNR is at least -1 dB. Therefore, this hybrid OCDMA-FSO network is indeed a prospective alternative to deliver high-speed communication services to remote access networks with deficient fiber infrastructure.

Appendix: Symbols and notation

Symbol	Description
$\mathbf{A}$	$= \mathbf{DC}$
b	Binary data (b $\in \{0,1\}$)
$\mathbf{C}$	$N \times N$ positive definite correlation matrix ($= \sqrt{\mathbf{C_y}}$)
c_{mi}	Coefficient from a partial fraction expansion procedure
$\mathbf{C_y}$	$N \times N$ channel correlation matrix
$C_1(t)$	Encoded transmitted signal of the desired user
$\mathbf{D}$	$N \times N$ diagonal matrix with the entries β for $i = 1 \ldots N$
d_i	$= -I/\lambda_i$
F	Total number of available wavelengths
I	Normalized optical irradiance
I_I	Total MAI given by the sum of the interferences from all users

Optics EXPRESS

I_{rx}	Total received optical irradiance
$I_{rx,i} = X_i Y_i$	Optical irradiance component received by the single aperture i, with $i = 1 \dots N$
L	Length of the code sequence
N	Number of aperture receiver lenses
N'	Number of different eigenvalues of matrix $\mathbf{A}$
$\mathscr{P}$	Probability of interference between the desired user and an interfering user
$r(t)$	Received signal at the input of the decoder
T_b	Bit period
T_c	Chip duration of all users' codes
U	Total number of simultaneous users in the network
V	$= \sum_{i=1}^{N} Y_i$
W	Weight of the code sequence
X	$\sim \mathscr{G}(\alpha_x, \beta_x)$
X_i	Large-scale irradiance fluctuations observed by the ith aperture and following a gamma distribution. $X_i = X, \forall i = 1 \dots N$.
Y_i	Small-scale irradiance fluctuations observed by the ith aperture and following a gamma distribution.
Z	Decision variable at the matched filter output
α	Effective number of small-scale cells of the scattering process
α_x	Effective number of large-scale cells of the scattering process
β	$= 1/\alpha$
β_x	$= 1/\alpha_x$
ξ	Zero-mean AWGN
η	Mean value of the MAI (=$(U-1)\mathscr{P}$)
$\{\lambda_i\}_{i=1}^{N}$	Eigenvalues of the matrix $\mathbf{A}$
ρ_{ij}	Correlation coefficient between ith and jth receiver apertures
μ	Optimum threshold ($\mu = W + \eta$)
$\mu_A(\cdot)$	Algebraic multiplicity
σ^2	MAI variance
σ_I^2	Normalized irradiance variance
σ_N^2	Total noise power in detector current
ζ	Signal-to-interference ratio

Acknowledgments

This work was supported by the Andalucía Talent Hub Program launched by the Andalusian Knowledge Agency, co-funded by the European Union's Seventh Framework Program, Marie Curie actions (COFUND - Grant Agreement no 291780), the HOT project of Danish Innovation Fund, the Marie Curie FENDOI project, the Ministry of Economy, Innovation, Science and Employment of the Junta de Andalucía and the Brazilian agencies CAPES, CNPq, and FAPESP.